Influence of wetting-layer wave functions on phonon-mediated carrier capture into self-assembled quantum dots

Markussen, Troels; Kristensen, Philip Trøst; Tromborg, Bjarne; Berg, Tommy Winther; Mørk, Jesper

Published in:
Physical Review B Condensed Matter

Link to article, DOI:
10.1103/PhysRevB.74.195342

Publication date:
2006

Document Version
Publisher's PDF, also known as Version of record

Influence of wetting-layer wave functions on phonon-mediated carrier capture into self-assembled quantum dots

Troels Markussen, Philip Kristensen, Bjarne Tromborg, Tommy Winther Berg, and Jesper Mørk*
Research Center COM, NanoDTU, Technical University of Denmark, DK-2800 Kgs. Lyngby, Denmark
(Received 28 April 2005; revised manuscript received 8 August 2006; published 30 November 2006)

Models of carrier dynamics in quantum dots rely strongly on adequate descriptions of the carrier wave functions. In this work we numerically solve the one-band effective mass Schrödinger equation to calculate the capture times of phonon-mediated carrier capture into self-assembled quantum dots. Comparing with results obtained using approximate carrier wave functions, we demonstrate that the capture times are strongly influenced by properties of the wetting layer wave functions not accounted for by earlier theoretical analyses.

DOI: 10.1103/PhysRevB.74.195342 PACS number(s): 78.67.Hc, 73.63.Kv

I. INTRODUCTION

Size quantization in artificial quantum dots leads to the possibility of controlling the available states of a material, thus fundamentally influencing its electronic and optical properties.[1] Today, semiconductor quantum dot materials have, e.g., been used to improve the properties of semiconductor lasers[2] as well as optical amplifiers.[3] Stranski-Krastanow cystal growth is the most common method of realizing quantum dot materials.[1] This method produces so-called self-assembled quantum dots (QDs) consisting of nanometer sized protrusions on a thin wetting layer (WL). In optoelectronic applications of quantum dots, e.g., for lasers and optical amplifiers, carriers are injected into the continuum (reservoir) states of the wetting layer, and subsequently relax into the bound quantum dot states. The time scale of this so-called carrier capture relaxation process is very important for the applications; a long capture time thus limits the modulation response of lasers[4] as well as the output power of amplifiers.[5] Understanding the dependence of the capture time on the dot-wetting layer geometry as well as the material parameters is therefore of significant interest for describing the dynamics of such devices and suggesting improved designs.

The capture process has been studied experimentally as well as theoretically and has contributions from carrier-carrier (Auger) as well as carrier-phonon scattering.[6–14] Typically, capture times in the range of a few to several tens of picoseconds are measured. Theoretically, the capture rate depends on matrix elements involving wave functions corresponding to initial extended (continuum) states in the wetting layer and final bound (discrete) states of the quantum dot. While the discrete bound state wave functions are usually found by solving the effective mass Schrödinger equation in the full potential (including the dot), the continuum wave functions are constructed using different approximations, including simple plane waves.[12] The plane wave approximation, however, does not take into account the influence of the QD potential on the extended states, thus excluding effects due to scattering off the dot potential, such as the existence of quasibound states. To remedy this problem, the use of so-called orthogonalized plane waves has been suggested.[15] This more elaborate approach uses linear combinations of plane waves and bound states to create wave functions that are orthogonal to the bound dot states.[6,11,14,15] In this paper we present the results of capture time calculations using numerically computed wave functions that take into account the full dot and wetting layer potential. By comparing to the cases of simple approximate wetting layer descriptions, we show that the detailed form of the wetting layer wave functions strongly affects the absolute value of the capture time as well as its qualitative variation with dot size. Also we demonstrate that the orthogonalized plane waves method need not result in any improvement of the capture times calculated. We specifically consider a rotationally symmetric model of a self-assembled QD (Ref. 16) and limit ourselves to the case of single-phonon-mediated carrier capture. We do not consider contributions to the capture rate from Auger processes and many-body effects, as the focus of the paper is on how the chosen wave functions affect the calculated capture times. However, a comprehensive many-body approach would also rely on the use of appropriate single particle eigenstates;[17] so the results may have wider implications than just for the carrier capture problem considered. Exploiting the rotational symmetry, the problem of solving the Schrödinger equation is reduced to two dimensions, making a finite element method (FEM) efficient. In this rotational symmetry it is convenient to work with a basis set of Bessel functions (BF), rather than the usual plane waves representing free carriers in a WL without any QD. Similarly, the orthogonalization method of Refs. 14 and 15 here translates into the use of a set of orthogonalized Bessel functions (OBF).

The paper is organized as follows: Section II presents the theory, including the dot and wetting layer geometry considered. The various descriptions of the wetting layer states are presented and the expression for the carrier capture rate is derived. Numerical results for the capture time are presented in Sec. III, including its variation with dot radius and a detailed comparison between the different wetting layer descriptions. Finally, Sec. IV summarizes the main findings.

II. THEORY

A. Mathematical model

The rate of capture of an electron from the wetting layer into a bound QD state depends on the envelope wave func-

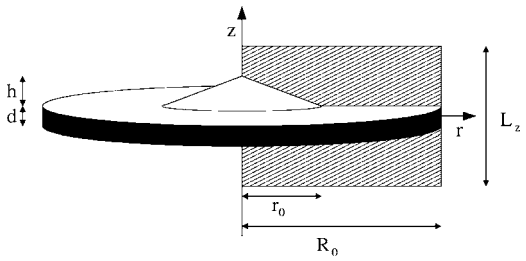

FIG. 1. Schematic of a quantum dot in the form of a cone on top of a wetting layer. The rotationally symmetric model allows for an efficient two-dimensional numerical solution.

tions of the WL as well as the QD electrons. We shall use a one-band approximation for the conduction band electrons and ignore the effects of band mixing as well as the mass anisotropy caused by strain in the wetting layer and the QD. The envelope wave functions are therefore assumed to be solutions to

$$-\frac{\hbar^2}{2}\nabla\cdot\left(\frac{1}{m^*(\mathbf{r})}\nabla\Psi(\mathbf{r})\right)+V(\mathbf{r})\Psi(\mathbf{r})=E\Psi(\mathbf{r}) \qquad (1)$$

with the potential, $V(\mathbf{r})$, and the effective mass, $m^*(\mathbf{r})$, being, in general, functions of the three spatial coordinates, and E being the eigenenergy. Following the ideas of Ref. 16 we simplify the QD geometry by considering a single, conical dot atop a wetting layer of the same material and embedded in a different bulk material. The model is shown in Fig. 1. The QD base radius is r_0, h is the height of the QD and d is the wetting layer thickness. R_0 and L_z define the radius and the height of the normalization volume. In this approximation the potential experienced by carriers in the wetting layer will be rotationally symmetric, depending only on the radial distance r and the vertical position z. The reduction of the effective mass Schrödinger equation to a two-dimensional problem allows for an efficient solution using numerical methods. To this end we assume a separable form for the solutions

$$\Psi(r,z,\phi)=\varphi(r,z)e^{im_z\phi},\quad m_z\in Z \qquad (2)$$

with m_z being the magnetic quantum number and the functions $\varphi(r,z)$ being the solutions to the eigenvalue equation

$$\left[-\frac{\hbar^2}{2r}\frac{\partial}{\partial r}\left(\frac{r}{m^*}\frac{\partial}{\partial r}\right)-\frac{\hbar^2}{2}\frac{\partial}{\partial z}\left(\frac{1}{m^*}\frac{\partial}{\partial z}\right)+V(r,z)+\frac{m_z^2\hbar^2}{2m^*r^2}\right]\varphi(r,z)=E\varphi(r,z). \qquad (3)$$

B. Descriptions of WL states

Throughout the work, the bound QD states, $|d_n\rangle$, have been calculated numerically using a finite element approach on the full potential in Fig. 1 (including the dot), whereas three different methods have been used in describing the continuum of WL states: a direct numerical calculation and two different approximations that have been used in the litterature so far. Below we discuss the three descriptions.

1. Finite element method

Numerical solution of the problem is carried out using the commercial FEM package FemLab[18] providing efficient mesh generation and eigensolvers. In numerically solving Eq. (3) we need to apply appropriate boundary conditions for the domain in Fig. 1. From Eq. (2) it is evident that any solution having magnetic quantum number $m_z\neq 0$ must be zero at $r=0$, and by demanding differentiability at $r=0$ one finds that the solutions corresponding to $m_z=0$ must have zero slope at $r=0$. Furthermore, we expect the eigenfunctions to exhibit an exponential decay in the bulk material away from the wetting layer, tending to zero at large distances. The application of a boundary condition at $r=R_0$ implies a quantization of the WL continuum. Effectively, this means that we only perform a discrete sampling of the WL states. As R_0 tends to infinity the energy spacing between the eigenfunctions tends to zero, and so, without loss of generality, we can set the eigenfunctions to zero at this boundary as well, in accordance with the boundary conditions of the bound state solutions. For the boundary at $r=0$ we thus have

$$\varphi(0,z)=0,\quad m_z\neq 0$$

$$\left.\frac{\partial\varphi}{\partial r}\right|_{r=0}=0,\quad m_z=0$$

while for all other boundaries we have

$$\varphi(R_0,z)=\varphi(r,L_z/2)=\varphi(r,-L_z/2)=0. \qquad (4)$$

2. Bessel function approximations

Previous works[12] have calculated carrier capture using wetting layer states described by plane waves, thus ignoring the influence of the dot potential on the free carriers. With no dot atop, the problem turns into the familiar problem of a quantum well with the potential and effective masses given as

$$V(z)=\begin{cases}0, & |z|\leqslant d/2,\\ V, & |z|>d/2,\end{cases}$$

$$m^*(z)=\begin{cases}m_w^*, & |z|\leqslant d/2,\\ m_b^*, & |z|>d/2,\end{cases}$$

where m_w^* and m_b^* denote the effective masses in the wetting layer and bulk region, respectively. We shall generally denote the solutions to Eq. (1) with the above potential as $|\mathrm{BF}\rangle$, defined as

$$\langle\mathbf{r}|\mathrm{BF}\rangle=\langle\mathbf{r}|k_r,m_z\rangle=J_{m_z}(k_rr)e^{im_z\phi}Z(z) \qquad (5)$$

with J_{m_z} being the Bessel function of order m_z, and

$$Z(z)=\begin{cases}Ae^{-k_bz}, & z>d/2,\\ B\cos(k_wz)+C\sin(k_wz), & |z|\leqslant d/2,\\ De^{k_bz}, & z<-d/2\end{cases}$$

with the WL and bulk wave vectors being in general nontrivial functions of the effective masses as shown in the Ap-

pendix. For small values of k_w and k_b, corresponding to the energies considered in the present work, the variations are small and we have used a constant effective mass. Also, at these energies, it suffices to include only the first subband having no nodes in the z direction.

C. Orthogonalized Bessel functions

The orthogonalized plane wave (OPW) method used in Ref. 14 is based on the assumption that there is a dense and random distribution of QDs with wave functions $|d_n\rangle$ which are spatially nonoverlapping when they belong to different QDs. From these localized wave functions one may construct a set of functions

$$|\mathbf{k}\rangle_o \equiv \left(|\mathbf{k}\rangle - \sum_n |d_n\rangle\langle d_n|\mathbf{k}\rangle\right) \Big/ N_{\mathbf{k}}, \tag{6}$$

where $|\mathbf{k}\rangle$ is the WL state with momentum $\mathbf{k}$ in the absence of QDs. The sum is over all QD states $|d_n\rangle$ within the normalization volume, and $N_{\mathbf{k}}$ is a normalization factor. It was shown in Ref. 14 that the functions in Eq. (6) are mutually orthogonal and also orthogonal to the QD wave functions, i.e., properties that are fulfilled by the exact WL wave functions. The set of functions in Eq. (6) are therefore called OPW functions. They can be expanded as

$$|\mathbf{k}\rangle_o = \sum_m (-i)^m e^{-im\theta}|k_r,m\rangle_o \tag{7}$$

where $|k_r,m\rangle_o$ is the orthogonalized Bessel function

$$|k_r,m\rangle_o \equiv \left(|k_r,m\rangle - \sum_n |d_n\rangle\langle d_n|k_r,m\rangle\right) \Big/ N_{\mathbf{k}}. \tag{8}$$

The discussion in this paper shows that the capture rate obtained by using OPW instead of the exact solutions is only a good approximation for small QDs.

D. Rate expression

The rate of carrier capture from an initial wetting layer state $|w\rangle$ to an empty QD state $|d\rangle$ by emission of a LO phonon can be approximated by Fermi's golden rule as[12]

$$R = \frac{2\pi}{\hbar}(\bar{n}+1)|\alpha_0|^2 \sum_w \left(\delta(E_d + \hbar\omega_{\mathrm{LO}} - E_w) f(E_w) \times \sum_\nu \frac{|\langle d|\psi_\nu^*(\mathbf{r})|w\rangle|^2}{q_r^2+q_z^2}\right), \tag{9}$$

with

$$|\alpha_0|^2 = e^2 \frac{\hbar\omega_{\mathrm{LO}}}{2\epsilon_0\epsilon^*}. \tag{10}$$

The expression is based on the Fröhlich Hamiltonian for the electron LO-phonon interaction. The sums in Eq. (9) run over $w=(k_r,m_w)$ and $\nu=(q_r,q_z,m_{ph})$, where m_w, m_{ph} are the magnetic quantum numbers for the WL electron and phonon, and q_r, q_z are the radial and transverse momenta of the phonon. The LO phonon is assumed to be dispersionless with energy $\hbar\omega_{\mathrm{LO}}$. The average number of phonons is given by $\bar{n}=(\exp(\hbar\omega_{\mathrm{LO}}/k_BT)-1)^{-1}$. In Eq. (10) ϵ_0 is the vacuum permitivity constant and $(\epsilon^*)^{-1}=\epsilon_\infty^{-1}-\epsilon_r^{-1}$, ϵ_r (ϵ_∞) being the static (high frequency) dielectric constant. The wave function of the emitted phonon is given as

$$\psi_\nu(\mathbf{r}) = bJ_m(q_r r)e^{iq_z z}e^{im\phi}, \tag{11}$$

where b is a constant which normalizes $\psi_\nu(\mathbf{r})$ in the normalization volume. Using the general form for the solutions in Eq. (2), it is evident that the matrix element in Eq. (9) fulfills the identity

$$\langle d|\psi_\nu^*(\mathbf{r})|w\rangle = bM_{d,w}\delta_{m_d+m_{ph},m_w} \tag{12}$$

with m_d being the magnetic quantum number of the QD state and

$$M_{d,w} = 2\pi \int \varphi_d^*(r,z)J_{m_w-m_d}(q_r r)e^{-iq_z z}\varphi_w(r,z)rdrdz.$$

The sums in Eq. (9) can be converted into integrals by introducing the corresponding densities of states. Using $b^2=q_r/(2R_0L_z)$, the expression (9) reduces to

$$R = \frac{(\bar{n}+1)|\alpha_0|^2R_0}{\pi^2\hbar} f(\tilde{E})\frac{1}{2k_r}\frac{dk_r^2}{dE} \times \sum_{m_w} \int\int_0^\infty dq_r dq_z \frac{q_r|M_{d,w}|^2}{q_r^2+q_z^2}, \tag{13}$$

where $M_{d,w}$ and dk_r^2/dE are derived for $E_w=\tilde{E}\equiv E_d+\hbar\omega_{\mathrm{LO}}$. Note that the expression above gives the rate of capture into a bound state with a given spin. The apparent dependence on the radius of the normalization volume R_0 vanishes since the wetting layer electron states $|w\rangle$ are normalized. Finally, the capture times, τ, are calculated from the capture rate as $\tau=1/R$.

If we use the OPW functions Eq. (6) for the WL states $|w\rangle$ in Eq. (9) it is only the OBF states that contribute since

$$\langle d|\psi_\nu^*(\mathbf{r})|\mathbf{k}\rangle_o = \langle d|\psi_\nu^*(\mathbf{r})|k_r,m_d+m_{ph}\rangle_o. \tag{14}$$

Furthermore, since the QDs are assumed to be nonoverlapping it is only the sum over states of the considered QD that needs to be included in Eq. (8). The energy E_w of the state $|\mathbf{k}\rangle_o$ is taken to be that of the plane wave as in the OPW method.

The use of Fermi's golden rule implies a perturbative approach for evaluating the effects of electron-phonon coupling, thus assuming weak coupling and a continuum of interacting states. However, it has been pointed out that these assumptions may be invalidated when considering the interaction of discrete electronic states in quantum dots with phonons,[10,19] in which case one should rather describe the excitations in terms of polarons. This is particularly important when both the initial and final electronic states are discrete[10] or have a resonant characteristic, as in the case of capture from a quasibound state in the wetting layer.[20] Recent numerical results of a quantum kinetic description of carrier-phonon interactions also indicate an important role of polarons on the process of carrier capture from continuum wetting layer states.[21] Still, those simulations use wetting layer wave functions described by orthogonalized plane wave states, which is an underlying assumption that needs to

be investigated. The combination of the many-body approach with the use of correct wetting layer wave functions is, however, outside the scope of this paper.

III. RESULTS

A. Capture time calculations

Throughout the work, unless otherwise noticed, parameters are assigned the following values: $V=697$ meV, corresponding to the energy difference in the conduction bands of an InAs wetting layer in a GaAs bulk as used in Ref. 16. Effective masses have the values $m_w^*=0.027m_0$ and $m_b^*=0.0665m_0$ (m_0 being the free electron mass) and correspond to those listed in Ref. 1. The phonons are assumed to be nondispersive, having the energy $\hbar\omega_{\mathrm{LO}}=35$ meV in accordance with the value used by Ref. 12. In calculating the Fermi function in Eq. (13) we have assumed a constant WL carrier density $n=10^{11}$ cm^{-2}. The parameters characterizing the geometry are $R_0=400$ nm, $L_z=60$ nm and the ratio of dot base radius to height is kept constant at $r_0/h=4.62$ as in Ref. 16. We have carried out calculations for WL thicknesses of $d=2$ nm and $d=4$ nm, corresponding to Refs. 14 and 16. For small values of k_w, corresponding to the energies in the present work, the variations in the effective mass, as discussed in the Appendix, are small and we have used a constant effective mass. The values used in the calculations are $m^*=0.0343m_0$ ($d=2$ nm) and $m^*=0.0295m_0$ ($d=4$ nm).

Using Femlab, the bound dot state is found as well as the relevant continuum wetting layer state having an energy closest to $\tilde{E}=E_d+\hbar\omega_{\mathrm{LO}}$. Note that the finite value of R_0 results in a discrete sampling of wetting layer energies, in general not including $\tilde{E}$. However, the large value of R_0 used in calculations minimizes the error made in choosing the numerical solution closest to $\tilde{E}$. The value of L_z used in calculations is large enough that the error made when invoking the Dirichlet boundary conditions at $z=\pm L_z/2$ is negligible. In general it has been tested that the numerical solutions have converged for the chosen values of the numerical parameters. In practical calculations, the contribution to the capture rate from WL states of different m_z converges rapidly to zero, so that it suffices to calculate rates from WL states having $|m_z|\lesssim 10$. This demonstrates the efficiency of fully utilizing the rotational symmetry in the calculations.

Figure 2 shows the calculated energies of the bound states as function of QD radius, r_0. The zero point of the energy is taken as the bottom of the InAs conduction band. The solid lines are for a wetting layer thickness $d=2$ nm while the dashed lines correspond to $d=4$ nm. Squares and circles indicate $m_z=0$ and $m_z=1$, respectively. The uppermost horizontal, dashed line indicates the lowest possible energy E_z of a wetting layer state ($d=2$ nm). The next line, displaced by $\hbar\omega_{\mathrm{LO}}$ defines the energy range from which carriers can be captured into the dot by phonon interaction. The two lowest horizontal lines correspond to $d=4$ nm.

In Fig. 3 we show the radial probability, $P(r)=r|\varphi(r,z)|^2$, for the bound state in a dot of radius $r_0=6.25$ nm and WL thickness $d=2$ nm. It is evident that a substantial part of the electron is located outside the dot area. For decreasing dot

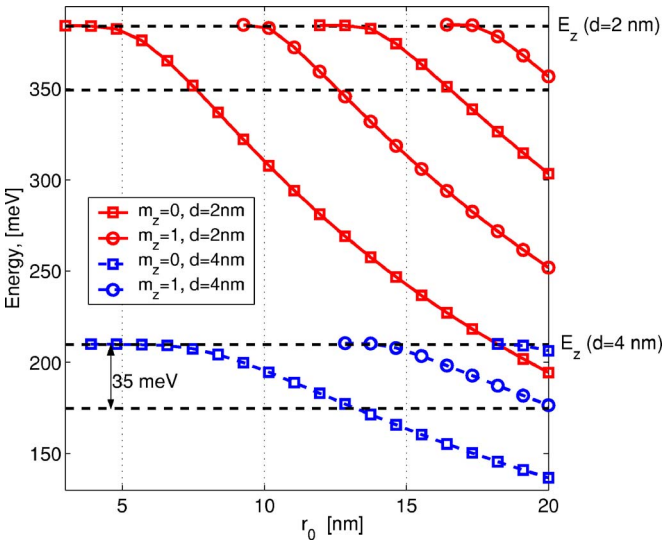

FIG. 2. (Color online) Energies of the bound states as function of QD radius, r_0. Solid lines denote wetting layer thickness $d=2$ nm while the dashed lines correspond to $d=4$ nm. The uppermost pair of horizontal, dashed lines define the interval in which capture can take place when $d=2$ nm, while the two lower lines correspond to $d=4$ nm.

sizes the electron is gradually squeezed out of the dot and eventually becomes unbound.

Figure 4 shows calculated capture times for dot radii $r_0\in[3.5;16]$. The wetting layer wave functions are determined numerically using Femlab. It is seen that there exist bands of dot radii where capture is energetically allowed, in accordance with previous results.[12] Generally the capture times increase at both ends of these bands. For small radii the reason is that the QD states extend more and more into the wetting layer, as mentioned above, and the matrix element in Eq. (13) tends to zero.

Enlarging the dot radius results in a lowering of the energy of the bound state, and thus a lowering of the energy of the relevant WL states. As the energy approaches the WL band edge, the WL state is expelled from the dot volume. It can be shown that the product $R_0|\varphi_w(r,z)|^2/k_r$ decreases as $[\ln(k_r r_0)]^{-2}$ in the dot region for $k_r\to 0$. The overlap between the WL state and the bound state becomes small, causing the

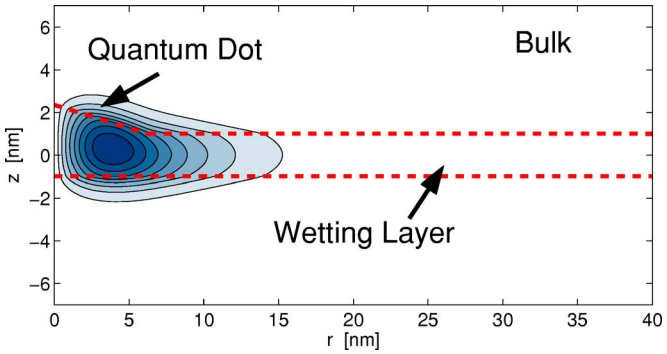

FIG. 3. (Color online) Radial probability density of the bound state at $r_0=6.25$ nm and $d=2$ nm. The state has energy $E=370$ meV.

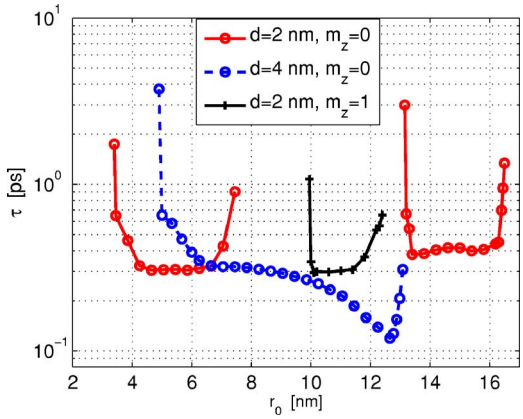

FIG. 4. (Color online) Capture times calculated with numerically determined wetting layer wave functions (FEM). Circles indicate capture to a bound state with $m_z=0$ and crosses to a state with $m_z=1$.

capture times to increase. We note that the increase is not due to depletion of the density of states as for a quantum dot in bulk material.[12] The degree to which the wetting layer states are displaced from the QD area depends on the specific geometry and on the nature of the relevant wetting layer states.

B. Comparison of WL descriptions

In Fig. 5 we compare capture times from the WL into the QD ground state ($m_z=0$) calculated using the three different descriptions (FEM, BF, and OBF). For small radii, $r_0 < 4.5$ nm, the calculated capture times are identical for the three WL descriptions, while for larger radii significant differences are observed. In the interval $4.5\ \text{nm} < r_0 < 6.5$ nm the capture times for the FEM solutions are almost constant. The OBF solutions give, on the other hand, capture times that increase with dot size in this range, whereas the capture times of the BF solutions decrease. For larger radii the FEM times increase due to the expulsion of the wetting layer states, as mentioned above. This expulsion effect is not accounted for by the BF approximation and only to some extent by the OBF approximation.

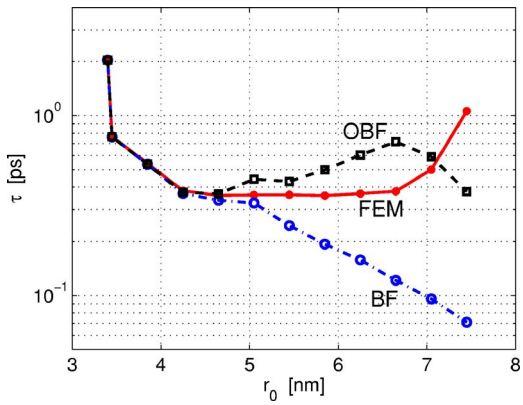

FIG. 5. (Color online) Capture times for WL thickness $d=2$ nm into the QD ground state ($m_z=0$), calculated with the three wetting layer descriptions (FEM, BF, and OBF)

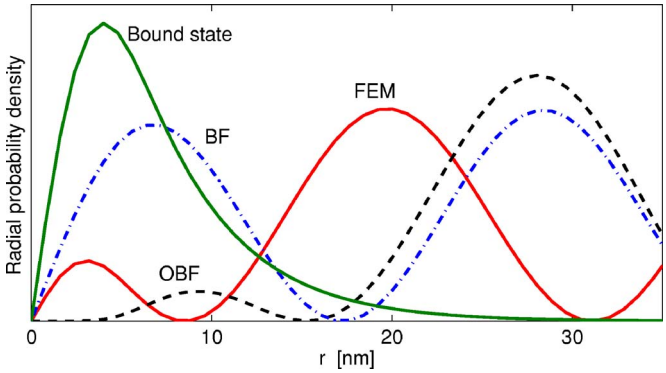

FIG. 6. (Color online) Radial probability densities (at $r_0=6.25$ nm and $z=0$ nm) for the QD state and the three WL states corresponding to magnetic quantum number $m_z=0$ and energies $E_w=E_{\text{dot}}+\hbar\omega_{\text{LO}}$.

Figure 6 shows radial probability densities (at $r_0=6.25$ nm and $z=0$ nm) for the QD state and the three WL states corresponding to magnetic quantum number $m_z=0$ and energy $\tilde{E}=E_d+\hbar\omega_{\text{LO}}$. The figure illustrates how the larger overlap between the BF and the QD state can explain the smaller capture times as compared to the OBF. Also, it illustrates that neither of the two approximations resembles the FEM solution. Although the $m_z=0$ wetting layer states contribute the most to the capture rate for this geometry, care should be taken since there are also contributions to the rate from wetting layer states with $m_z \neq 0$, cf. Eq. (13).

The reason for the intermediate decrease in capture times, seen for the FEM WL states (for $d=4$ nm) in Fig. 4, is evident from Fig. 2, showing the formation of a second band of bound QD states at $r_0 \approx 14$ nm ($d=4$ nm). At $r_0 < 14$ nm the increase in QD size affects the WL states by drawing them closer to the dot as r_0 is increased, eventually resulting in the second bound state. These nearly, or quasi, bound states have wave functions partially confined in space to the volume of the dot, resulting in larger matrix elements and smaller capture times. This may indeed be a situation in which Fermis golden rule may be violated due to strong coupling between the QD bound state and the quasibound state.[20] The actual capture times in this range of dot radii may therefore be inaccurate, but the effect of the quasibound states is clear. Both the BF and the OBF approximations fail to show this effect, since multiple scattering off the dot potential is neglected.

We emphasize that the OBF approximation in general does not seem to result in more accurate capture times than the BF approximation for larger radii. Nor is there any reason why it should, as the OBF wave functions are no closer to the true eigenstates of the Hamiltonian than are the BF wave functions.

IV. CONCLUSION

Calculations of phonon mediated carrier capture in self-assembled quantum dots have been carried out using the finite element method to obtain the electronic wave functions involved in the transitions. In this way capture times have

been calculated as a function of dot radius for two wetting layer thicknesses. These capture times have been compared to the results obtained using Bessel function solutions for the wetting layer without quantum dot as well as orthogonalized Bessel functions, corresponding to approaches taken in the literature so far.

The comparison has shown that neither of the two approximations lead to an accurate description valid in the full range of radii, each yielding approximately the same absolute error. The capture times for the finite element method solutions are found to increase rapidly at large radii. This reflects that wetting layer states with energies close to the band edge are squeezed out of the quantum dot area, a feature accounted for by neither the Bessel function nor the orthogonalized Bessel function approximations. We conclude that in general the calculations of the characteristic capture times for phonon mediated carrier capture from a wetting layer into a quantum dot depend critically on the approximations used for the wetting layer wave functions.

ACKNOWLEDGMENTS

Support by the IST EU projects "BIGBAND" and "DOTCOM" is gratefully acknowledged.

APPENDIX

The WL and bulk wave vectors are in general given as

$$\hbar k_w = \sqrt{2m_w^* E - \hbar^2 k_r^2},$$

$$\hbar k_b = \sqrt{2m_b^*(V-E) + \hbar^2 k_r^2}. \tag{A1}$$

From the symmetry of the problem it follows that two sets of solutions exist corresponding to symmetric (in the z direction) and antisymmetric modes, respectively. Demanding continuity and differentiability at the $z=\pm d/2$ boundary leads to the conditions

$$\frac{m_w^* k_b}{m_b^* k_w} = \tan\theta, \quad \text{symmetric modes } (C=0),$$

$$-\frac{m_w^* k_b}{m_b^* k_w} = \cot\theta, \quad \text{antisymmetric modes } (B=0),$$

where $\theta = \frac{k_w d}{2}$. In calculations of the rate of carrier capture the density-of-states factor dE/dk_r^2 enters. From the above equations and Eqs. (A1) it follows that

$$\frac{dE}{dk_r^2} = \frac{\hbar^2}{2m_w^* m_b^*} \frac{(m_w^*)^2 \cos^2\theta + (m_b^*)^2(\sin^2\theta + \theta\tan\theta)}{m_w^* \cos^2\theta + m_b^*(\sin^2\theta + \theta\tan\theta)}. \tag{A2}$$

This can be written in the form

$$\frac{dE}{dk_r^2} = \frac{\hbar^2}{2m^*(k_w)} \tag{A3}$$

which defines the effective mass $m^* = m^*(k_w)$ as a nontrivial function of the wave number in the wetting layer, k_w. For the special case of $m_b^* = m_w^* = m^*$ we recover the well-known relation $dE/dk_r^2 = \hbar^2/2m^*$.

By Eq. (A1),

$$\hbar^2(k_w^2 + k_b^2) = 2m_b^* V - 2(m_b^* - m_w^*)E, \tag{A4}$$

i.e., there are no WL subbands for

$$E \geqslant \frac{m_b^* V}{m_b^* - m_w^*}. \tag{A5}$$

This causes an effective mass dispersion, which becomes stronger for smaller WL thickness.

*Electronic address: jm@com.dtu.dk

[1] D. Bimberg, M. Grundmann, and N. Ledentsov, *Quantum Dot Heterostructures* (Wiley, New York, 1999).
[2] J. P. Reithmaier and A. Forchel, IEEE J. Sel. Top. Quantum Electron. **8**, 1035 (2002).
[3] T. Akiyama, M. Ekawa, M. Sugawara, H. Sudo, K. Kawaguchi, A. Kuramata, H. Ebe, K. Morito, H. Imai, and Y. Arakawa, Opt. Fiber Commun. **8**, PDP12 (2004).
[4] D. G. Deppe and D. L. Huffaker, Appl. Phys. Lett. **77**, 3325 (2000).
[5] T. W. Berg and J. Mørk, IEEE J. Quantum Electron. **40**, 1527 (2004).
[6] U. Bockelmann and T. Egeler, Phys. Rev. B **46**, 15574 (1992).
[7] B. Ohnesorge, M. Albrecht, J. Oshinowo, A. Forchel, and Y. Arakawa, Phys. Rev. B **54**, 11532 (1996).
[8] M. Brasken, M. Lindberg, and J. Tulkki, Phys. Status Solidi A **164**, 427 (1997).
[9] A. V. Uskov, J. McInerney, and F. Adler, Appl. Phys. Lett. **72**, 58 (1998).
[10] T. Inoshita and H. Sakaki, Phys. Rev. B **56**, R4355 (1997).
[11] R. Ferreira and G. Bastard, Appl. Phys. Lett. **74**, 2818 (1999).
[12] I. Magnusdottir, A. V. Uskov, S. Bischoff, B. Tromborg, and J. Mørk, J. Appl. Phys. **92**, 5982 (2002).
[13] I. Magnusdottir, S. Bischoff, A. V. Uskov, and J. Mork, Phys. Rev. B **67**, 205326 (2003).
[14] T. R. Nielsen, P. Gartner, and F. Jahnke, Phys. Rev. B **69**, 235314 (2004).
[15] H. C. Schneider, W. W. Chow, and S. W. Koch, Phys. Rev. B **64**, 115315 (2001).
[16] R. V. N. Melnik and M. Willatzen, Nanotechnology **15**, 1 (2004).
[17] H. Dery, B. Tromborg, and G. Eisenstein, Phys. Rev. B **67**, 245308 (2003).
[18] www.comsol.com
[19] O. Verzelen, R. Ferreira, G. Bastard, T. Inoshita, and H. Sakaki, Phys. Status Solidi A **190**, 213 (2002).
[20] I. Magnusdottir, A. Uskov, R. Ferreira, G. Bastard, J. Mørk, and B. Tromborg, Appl. Phys. Lett. **81**, 4318 (2002).
[21] J. Seebeck, T. R. Nielsen, P. Gartner, and F. Jahnke, Phys. Rev. B **71**, 125327 (2005).